Mining Science, vol. 29, 2022, 33–52

www.miningscience.pwr.edu.pl

Mining Science

(Previously Prace Naukowe Instytutu Gornictwa Politechniki Wroclawskiej, ISSN 0370-0798)

ISSN 2300-9586 (print)
ISSN 2353-5423 (online)

Received December 17, 2021; Reviewed; Accepted August 2, 2022

NUMERICAL SIMULATION STUDY ON FIRE HAZARD OF A COAL MINE TRANSPORT ROADWAY

Shijie PENG[1], Zhian HUANG[1]*,
Ding Wen DONG[2]

[1] State Key Laboratory of High-Efficient Mining and Safety of Metal Mines, University of Science and Technology Beijing, Ministry of Education, Beijing 100083, China
[2] School of Safety Science and Engineering, Xi'an University of Science and Technology, Xi'an, Shaanxi Province, 710054, China

Abstract: Due to the special structures and geographical environments of the main transport roadway of underground coal mines, it is difficult to deal with accidents and rescues in cases of fire and it is easy to cause casualties and structural damage of the roadway. In this study, a roadway fire model was established using FDS software on the basis of theoretical analysis. The smoke diffusion, temperature distribution, and CO concentration distribution in a fire period were simulated under four working conditions. The results showed that the time required for the smoke layer to descend to human breathing height was positively correlated with the distance between the position and the fire source. Under the most unfavorable conditions, the smoke reached human breathing height at 15.11 s and 100 m away from the fire source. After the fire broke out, the ambient temperature in the roadway rose rapidly, and the highest temperature in the area adjacent to the fire source reached 340 ℃. The farther away from the fire source, the lower the temperature, but it was still higher than the human body's optimum temperature (25 ℃) until 200 m away. The results of this study can provide a basis for the preparation of roadway fire emergency plans.

Keywords: *mine fire, fire risk, numerical simulation, FDS, mine ventilation*

1. INTRODUCTION

In recent years, coal mine fire accidents have occurred frequently, and they cause significant property losses and casualties every year. Therefore, it is necessary to pre-

* Corresponding author: huang_za@qq.com (Z. Huang)

doi: 10.37190/msc222904

vent and control coal mine fires. Roadways are relatively closed areas. A previously reported accident analysis showed (Yang et al. 2011) that their internal lights are dark, driving on them is risky, and possibilities of fire are high. Roadway fires seriously threaten the safety of personnel. In addition, the internal diameters of roadways are small, and their visibility is low (Ingason 2015), which increases the difficulty of rescue. Therefore, reasonably analyzing fire risk and mastering the laws of roadway fire development will contribute to the implementation of emergency rescues.

Most experts and scholars have used numerical simulation methods to study actual fire problems (Perera et al. 2012). Model research, on the other hand, can allow for clear statistics and the direct analysis of specific physical parameters. Kochevsky (2004) reported that CFD software has a high accuracy in simulating multi-component, multi--phase, and compressible flows by combining CFD simulations with experiments. Chasko et al. (2005) focused on the reactions and escape methods of underground miners after mine fires. Yan et al. (2013) improved the CFD algorithm and proposed a new escape route planning method for underground mines using an algorithm. Hansen et al. (2013) conducted two comprehensive fire tests on mining vehicles in a mine and found that the peak heat release rates of a wheel loader and drilling rig were 15.9 and 29.4 MW, respectively. Roh et al. (2007) previously studied critical ventilation velocity for estimating different heat release rates through longitudinal ventilation. Hansen (2012; 2015; 2017; 2021) analyzed fire accidents and found that vehicles and mobile devices were the main fire sources of underground structures; he conducted two comprehensive fire tests on vehicles in underground structures and reported heat release rate curves of underground fires. Adjiski et al. (2005) simulated a mine, analyzed the fire situation, and established an optimal evacuation route through software. Ingason H. et al. (2010) explored the influence of cross-sectional area and ventilation on the heat release rate under longitudinal ventilation, and they estimated the heat release rate of roadway fires under different conditions. Wang et al. (2010) studied the influence of smoke generated by tunnel fires on the human body, and changed the smoke emission rate of an open tunnel in the experiment process to simulate different hazards caused by different smoke volumes. There have been few studies on the exogenous mine fire, especially when exogenous fire occurs the research on critical wind speed, smoke movement, temperature distribution and CO concentration distribution in transportation roadway is insufficient. Research on these topics are particularly important for how to carry out emergency rescues and minimize the harm of personnel when similar fires occur underground.

In this study, the transport roadway of a mine was used as the study object. Firstly, a theoretical model of numerical simulation was established. Then, according to the fire scenario and the requirements of fire selection (Hirai 2011), four working conditions were set for simulation according to the different wind speeds and HRR (heat release rates). The critical wind speed, flue gas spreading and falling law, temperature distribution, and CO concentration distribution law of roadway fires were analyzed.

The study results can provide a reference for the creation of roadway fire ventilation rescue schemes.

2. CALCULATION METHOD AND MODEL

For this chapter, a numerical simulation model of roadway fires was established, the boundary of the model was set, and numerical simulations of roadway fires were carried out. In Chapter 3, the risk of roadway fires is comprehensively evaluated according to the CO concentration distribution, temperature distribution, smoke diffusion law, and descending time distribution in the simulation results.

2.1. THE GOVERNING EQUATION

A turbulent flow model was established to simulate the flow law of roadway fire smoke. Generally, a large eddy numerical simulation (LES) (Mouilleau et al. 2009; Oka et al. 2020) is used to simulate turbulent behavior. After a fire, the smoke flow in a fire source tunnel is complicated due to the different temperatures around the fire source. The conservation of mass equation, component equation, energy equation, motion equation, and state equation – which constitute the basic equations of fluid motion (Shen et al. 2008; Ying et al. 2012) – were established according to the conservation of matter, energy, and momentum.

(1) Mass conservation equation:

$$\frac{\partial \rho}{\partial t} + \nabla \cdot \rho \mu = 0, \tag{1}$$

where:

ρ – gas density;
μ – dynamic viscosity of gas;
τ – burning time.

(2) Composition equation:

$$\frac{\partial}{\partial t}(\rho Y_i) + \nabla \cdot \rho D_i \nabla Y_i + m \cdot m_i, \tag{2}$$

where:

Y_i – mass fraction of the *i*-th component,
D_i – the diffusion coefficient of the *i*-th component,
m_i – mass formation rate per unit volume of the *i*-th component.

(3) Momentum conservation equation:

$$\rho\left(\frac{\partial \mu}{\partial t}+(\mu\cdot\nabla)\mu\right)+\nabla P=\rho g+\int+\nabla\tau, \tag{3}$$

where:

$\int$ – mass fraction of the *i*-th component,

P – the diffusion coefficient of the *i*-th component.

(4) Ideal gas equation of state:

$$\mathrm{p}=\frac{\rho RT}{\overline{W}} \tag{4}$$

where:

$\overline{W}$ – molecular mass of a gas,

T – temperature,

R – ideal gas constant.

(5) Energy conservation equation:

$$\frac{\partial}{\partial\tau}(pH)+\nabla\cdot\rho H\mu=\frac{\partial p}{\partial\tau}+\varphi+qm_i-\nabla\cdot q, \tag{5}$$

where:

H – sensible enthalpy,

q – heat release rate per unit volume,

φ – the dissipation function.

2.2. FIRE MODEL ESTABLISHMENT AND PARAMETER SETTING

2.2.1. ASSUMPTIONS AND SIMPLIFICATION OF THE MODEL

1) Before the fire, the airflow in a roadway is stable, the roadway wall is fixed without slip, and the wall temperature is constant.
2) The flue gas produced by combustion is regarded as a multi-component ideal gas, and there are no chemical reactions between flue gas components.
3) No chemical reaction occurs when the flue gas generated by combustion flows in a roadway downwind of the fire source.
4) The oxidant was considered sufficient, and the flue gases produced by combustion were mainly considered to be CO and CO_2 (Singh et al. 2007).

2.2.2. THE ESTABLISHMENT OF GEOMETRIC MODELS

In this study, a geometric roadway model was established by using PyroSim. The cross-sectional size ratio was 1:1. The specific parameters are listed in Table 1, and the section of roadway is shown in Fig. 1. The location of the fire source was set to 100 m away from the entrance of the selected area. The main combustion substances were $C_4H_{10}O$ and C_8H_{18}, the main products were set as CO_2, CO and H_2O, and the reaction type was set as Simple Chemistry. The main study area had a length of 400 m, a width of 4 m, and a height of 4 m downstream of the fire source. The geometric model of the roadway is shown in Fig. 2.

Table 1. Shape parameters of main tunnel

Parameter	Value [m]
Length of the roadway	500
The lateral width	4
Height of roadway	4
Thickness of supporting layer	0.8
Fire source location	100 m away from the air inlet

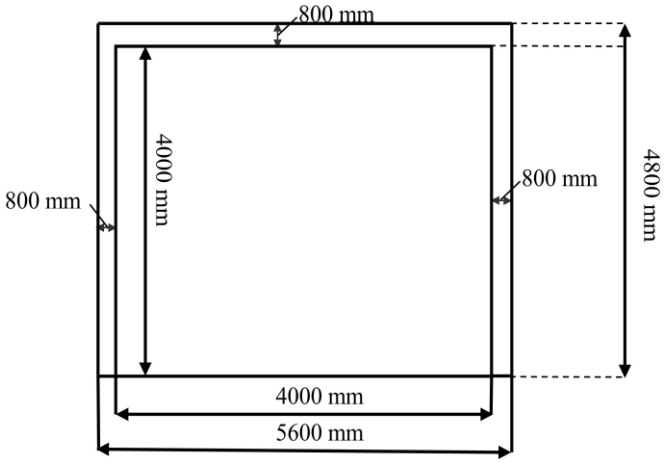

Fig. 1. Schematic diagram of main roadway section

In this study, 32 temperature detectors and 32 smoke detectors were set up in the geometric model to record the simulation results of temperature and smoke layer height, respectively. The location of the fire source is shown in Fig. 3.

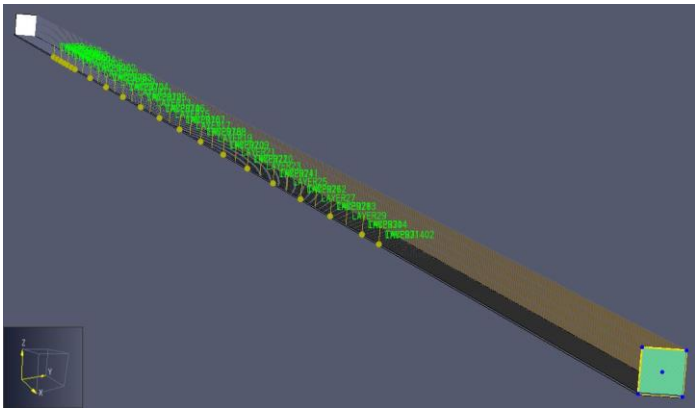

Fig. 2. Geometric model of roadway

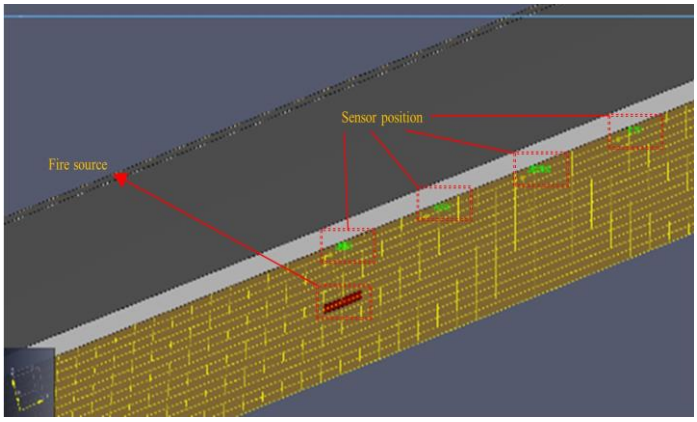

Fig. 3. Location of fire source in geometric model

There are two types of fire growth models: ①Steady state combustion, in which the heat release rate of the fire source is constant and does not change with time; ②unsteady combustion, which can be divided into three stages, i.e., the initial growth stage, the middle stage of stable combustion, and the end of decay stage. Of these, the second unsteady combustion fire growth model is more in line with the actual situation of tunnel fires. Therefore, following the fire heat release theory of Ingason et al. (2011), as well as a square growth model for the growth stages and an index model for the stable combustion and attenuation stages, a numerical simulation of the tunnel fire was carried out using the following approximation model:

$$Q = \alpha t^2, \tag{6}$$

where:

Q – fire power,

t – burning time,

α – fire growth factor.

Common fire growth types are shown in Table 2 (Ying et al. 2011). The growth factor is determined by the type of fire growth (slow, medium, fast and ultra-fast).

Table 2. Types of fire growth

Type	Slow	Medium	Fast	Ultra-fast
α [kW/s^2]	0.0029	0.0117	0.0470	0.1890

The fire growth type of this roadway is ultra-fast, and the fire growth coefficient of this roadway was set to α = 0.1890. In this study, after referring to the heat release rate of coal combustion (Ran et al. 2020), it was decided that the heat release rates of medium and large fires in the roadway were 10 and 20 MW, respectively. Medium-sized and large-sized fires required wind speeds of the flue gas countercurrent to be 2 and 4 m/s, respectively (Wang et al. 2011). According to formula (6), it can be seen that the total burning time was not less than T = 250 s for a medium-sized fire with a fire source power of 10 MW.

2.3. SETTING OF BOUNDARY CONDITIONS

The boundary conditions of the roadway were set as shown in Table 3.

Table 3. Boundary conditions of the underground mine roadway

Type	Surface material	Concrete temperature	Air inlet position
The boundary conditions	0.8 m of concrete	20 ℃	Model origin

When establishing the tunnel fire simulation geometric model, the grid division was calculated according to Eq. (7):

$$D^* = \left[b \frac{Q}{\rho_\infty C_p T_\infty \sqrt{g}} \right]^{\frac{2}{5}}. \tag{7}$$

Hexahedral cells were used in the grid, and the cell length was 1 m, i.e., a 1 m^3 space corresponded to a grid cell in this study. The length, width, and height of the tunnel area simulated in this model were 500, 4, and 4 m, respectively. Therefore, the

numbers of *X*, *Y*, and *Z* grid cells were set to 500, 4 and 4, respectively, and the model had 8000 grid cells in total.

2.4. FDS CALCULATION PROCESS

With the help of simulation software PyroSim, the FDS method was used for simulation analysis, and its workflow chart is shown in Fig. 4.

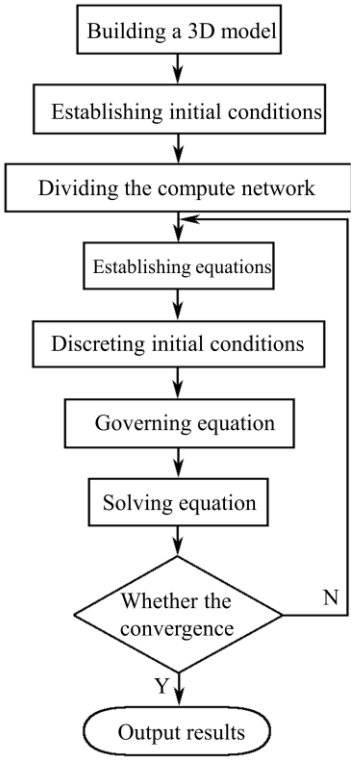

Fig. 4. FDS solution process

2.5. DETERMINATION OF FIRE CONDITIONS

In this study, different fire scales were selected by comprehensively considering types of roadway, the HRRs of roadway fires, ventilation wind speed, and other factors. Table 4 shows the four working conditions used in this study. The fire power of medium and large fires was selected as the working condition, and the wind speed was selected according to The Design and Planning System of Underground Hard Rock Mine (Kng et al. 2019).

Table 4. Setting of working conditions

The wind speed [m/s] Fire power [MW]	2	3
10	Working condition I	Working condition II
20	Working condition III	Working condition IV

3. NUMERICAL SIMULATION RESULTS AND ANALYSIS

3.1. SELECTION OF CRITICAL WIND SPEED

3.1.1. ESTIMATION OF CRITICAL WIND SPEED

Wind speed in a roadway is the key to controlling temperature, CO concentration, and smoke distribution when roadway fires occur (Morin et al. 2001). When the wind speed of longitudinal ventilation is lower than the critical wind speed, a flue gas countercurrent will occur (as shown in Fig. 5); otherwise, no countercurrent will occur when the wind speed of ventilation is higher than the critical wind speed. The backflow of flue gas can cause the air to carry a large amount of toxic and harmful substances (such as CO), and there is a risk of fire expansion. Therefore, it was necessary to simulate the critical wind speed of roadways in this study.

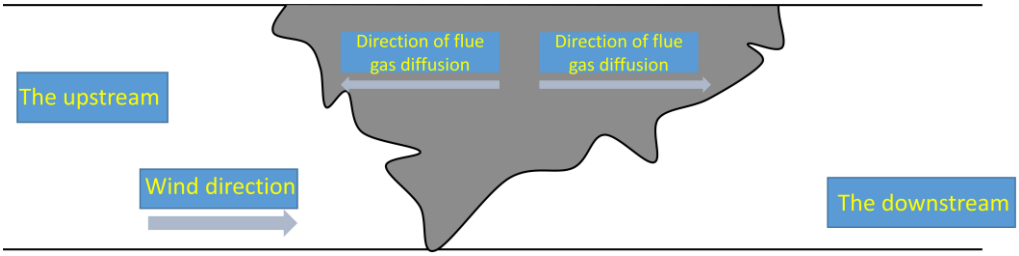

Fig. 5. Schematic diagram of flue gas reflux

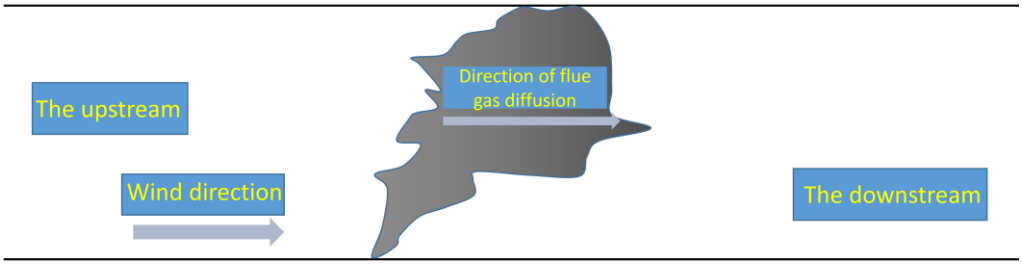

Fig. 6. Schematic diagram of flue gas without countercurrent

In general, critical wind speed has been found to be positively correlated with the scale of roadway fires, but critical wind speed does not infinitely increase with fire scale (Wang et al. 2002); this is because when the fire scale increases to a certain amount, the flame directly impacts the roof, thus leading to the weakening of the buoyancy effect of cold air and halting increases in the critical wind speed.

3.1.2. CRITICAL WIND SPEED FOR CONDITIONS I AND II

The fire scale was set to a 10 MW medium fire, the ventilation wind speeds were set to 2 and 2.5 m/s, and the total simulation time was set to 600 s. After the calculation, the results of smoke flow were observed in Smokeview. Figures 7 and 8 show the calculation results of T = 5, 60, and 300 s.

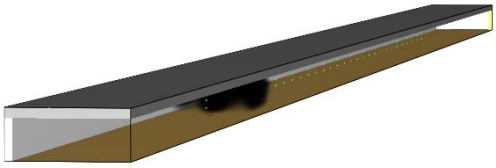

a) T = 5 s

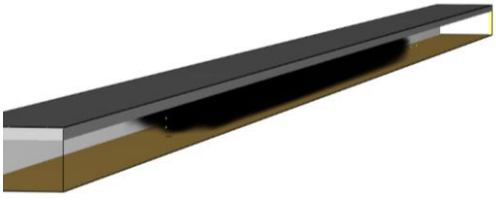

b) T = 60 s

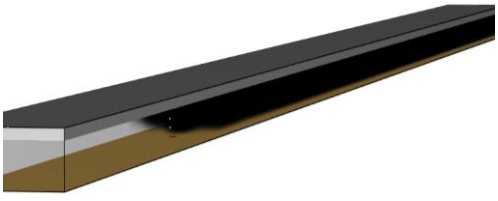

c) T = 300 s

Fig. 7. Flue gas distribution when wind speed is 2 m/s

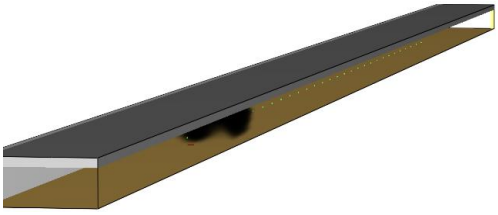

a) T = 5 s

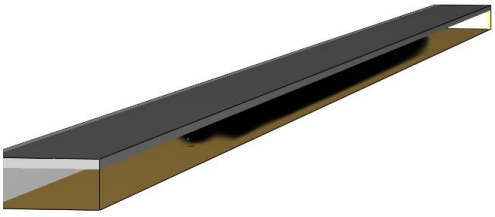

b) T = 60 s

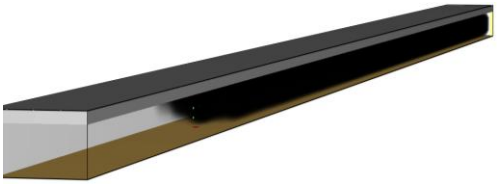

c) T = 300 s

Fig. 8. Flue gas distribution when wind speed is 2.5 m/s

According to the results shown in Figs. 7 and 8, when the supply wind speed of 2.5 m/s was used, the direction of flue gas flow was basically consistent with the direction of wind speed, that is, there was no significant countercurrent phenomenon. Therefore, it can be judged that a wind speed of 2.5 m/s may have been greater than the critical wind speed. However, when the supply wind speed of 2 m/s was selected, the flue gas tended to flow in the direction opposite to the ventilation direction, so the wind speed was less than the critical wind speed. The dichotomy method was adopted to continue the simulation with a supply wind speed of 2.3 m/s. The simulation results showed that when the supply wind speed was
2.3 m/s, the flue gas just did not reverse flow. Therefore, the critical wind speed could be regarded as 2.3 m/s when a medium-sized fire scale of 10 MW occurred in the roadway.

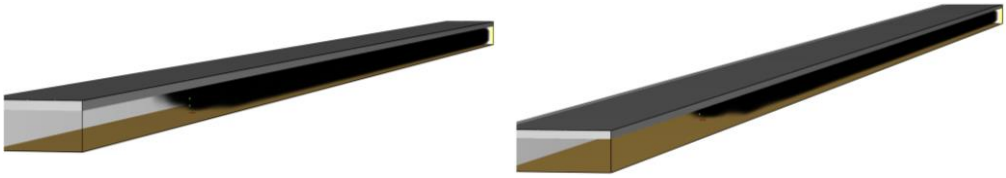

a) Flue gas distribution when wind speed is 2.2 m/s

b) Flue gas distribution when wind speed is 2.3 m/s

Fig. 9. Determination of critical wind speed when the fire scale reaches 10 MW

3.1.3. CRITICAL WIND SPEED OF CONDITIONS III AND IV

The fire scale was set to a 20 MW large fire, the ventilation wind speeds were set to 3 m/s and 3.5 m/s, and the total simulation time was set to 600 s. After the calculation, the detailed results of smoke flow were observed in Smokeview. Figures 10 and 11 show the calculation results of T = 5, 60, and 300 s.

According to the results shown in Figs. 10 and 11, when the supply wind speed was 3.5 m/s, the direction of flue gas flow was basically consistent with the direction of wind speed, that is, there was no significant countercurrent phenomenon. Therefore, it can be judged that the wind speed of 3.5 m/s may have been greater than the critical wind speed. However, when the wind speed was 3.0 m/s, there was a relatively obvious smoke reflux phenomenon, so the wind speed was small. The dichotomy method was used to continue the simulation with supply wind speeds of 3.3 and 3.1 m/s. The simulation results showed that the flue gas did not reverse flow when the wind speed was 3.1 m/s. Therefore, the critical wind speed of the 20 MW roadway fire could be regarded as 3.1 m/s.

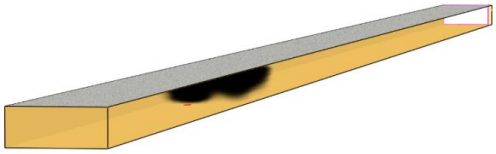

a) T = 5 s

b) T = 60 s

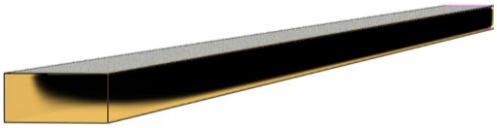

c) T = 300 s

Fig. 10. Flue gas distribution when wind speed is 3 m/s

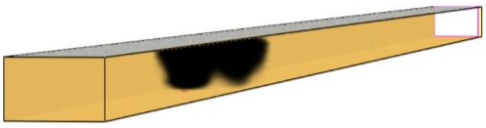

a) T = 5 s

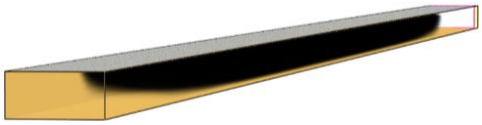

b) T = 60 s

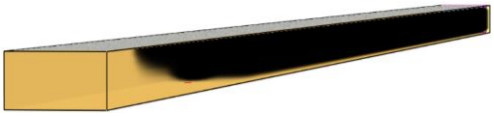

c) T = 300 s

Fig. 11. Flue gas distribution when wind speed is 3.5 m/s

a) Flue gas distribution when wind speed is 3.0 m/s

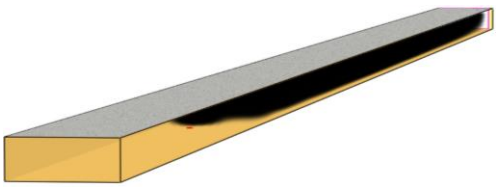

b) Flue gas distribution when wind speed is 3.1 m/s

Fig. 12. Determination of critical wind speed when the fire scale reaches 20 MW

3.2. SMOKE SPREAD RESULT

The fire source was placed 100 m away from the entrance of the roadway, and smoke detectors were set at 101, 105, and 110 m, followed by one every 10 m until 300 m. A total of 32 smoke detectors were placed 1.8 m above the ground to monitor the smoke situation. These four working conditions were simulated, and the combustion duration was set to 1800 s. The following figure shows the smoke movement of 60 s, 300 s, 600s, 1200 s, 1800 s and other key nodes.

3.2.1. SIMULATION RESULTS OF OPERATING CONDITION I

The smoke diffusion results at 60, 300, 600, 1200, and 1800 s following a roadway fire under working condition I are shown in Fig. 13.

a) T = 60 s

b) T = 300 s

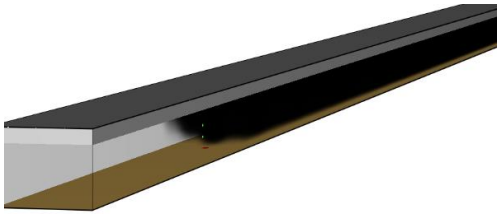

c) T = 600 s

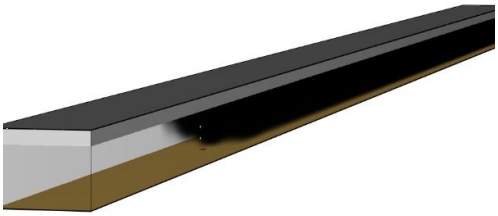

d) T = 1200 s

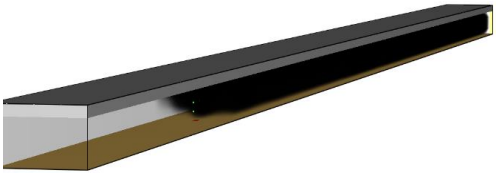

e) T = 1800 s

Fig. 13. Smoke diffusion diagram under working condition I

3.2.2. SIMULATION RESULTS OF OPERATING CONDITION II

Smoke diffusion results at 60, 300, 600, 1200, and 1800 s following a roadway fire under working condition II are shown in Fig. 14.

a) T = 60 s

b) T = 300 s

c) T = 600 s

d) T = 1200 s

e) T = 1800 s

Fig. 14. Smoke diffusion diagram under working condition II

3.2.3. SIMULATION RESULTS OF OPERATING CONDITION III

Smoke diffusion results at 60, 300, 600, 1200, and 1800 s following a roadway fire under working condition III are shown in Fig. 15.

a) T = 60 s

b) T = 300 s

c) T = 600 s

d) T = 1200 s

e) T = 1800 s

Fig. 15. Smoke diffusion diagram under condition III

3.2.4. SIMULATION RESULTS OF OPERATING CONDITION IV

Smoke diffusion results at 60, 300, 600, 1200, and 1800 s following a roadway fire under working condition IV are shown in Fig. 16.

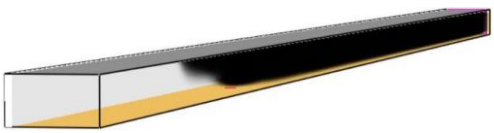

a) T = 60 s

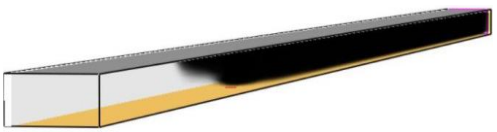

b) T = 300 s

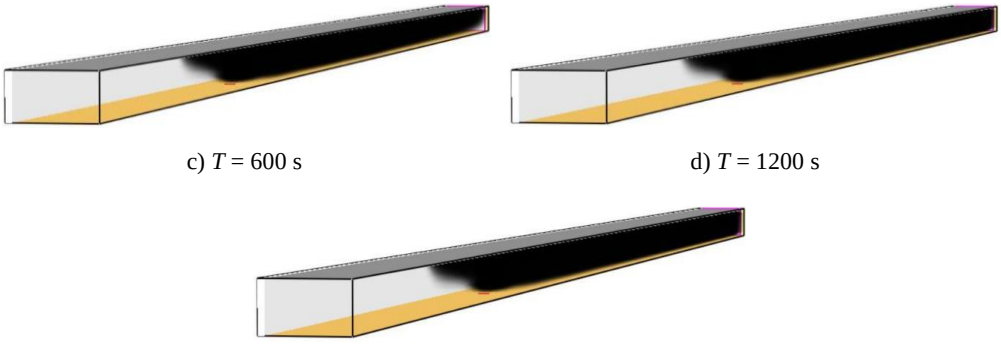

c) T = 600 s d) T = 1200 s

e) T = 1800 s

Fig. 16. Smoke diffusion diagram under condition IV

3.2.5. FLUE GAS FALL TIME

Smoke is usually the biggest disaster-causing factor in statistically analyzed fire accidents, accounting for about 80% of deaths caused by fire accidents (Bakhtiyari et al. 2017). After the flue gas is produced, it slowly moves down and reach a height of about 1.8 m to be absorbed by the human body. In order to calculate the time required for flue gas to settle to the breathing height of personnel (set to 1.8 m in this study) under various working conditions, the simulation duration was set to T =1800 s. Flue gas layer falling times at different positions of the roadway are shown in Fig. 17.

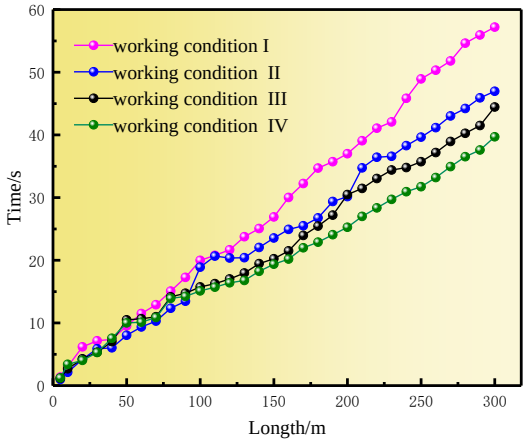

Fig. 17. Statistical diagram of time required for flue gas drop

Figure 17 shows a statistical chart of the time required for flue gas descent. According to the comparison of the four working conditions, it can be seen that the flue gas falling time was positively correlated with the distance between the position and the

fire source, and the longer the distance, the longer the flue gas falling time. Secondly, there was a negative correlation between the flue gas falling time and the supply wind speed, and large longitudinal ventilation hindered the flue gas falling time. Finally, the smoke descent time was also shown to be related to the fire scale. The larger the fire scale, the less time needed for the smoke descent. Under the most unfavorable conditions, the smoke reached the breathing height of the human body at 15.11 s and 100 m away from the fire source.

3.3. ANALYSIS OF FIRE TEMPERATURE FIELD

When studying the temperature distribution, the Y = 2.0 section of the model was set as a temperature-detection surface. At the same time, we added a group of 32 temperature detectors placed at 1, 5, and 10 m away from the fire source, as well as every 10 m after. The temperature distribution of the middle line of roadway was analyzed with these detectors. This section presents an analysis of the operation results of the four different working conditions set above. The results of temperature simulation in the four working conditions are shown in Fig. 18.

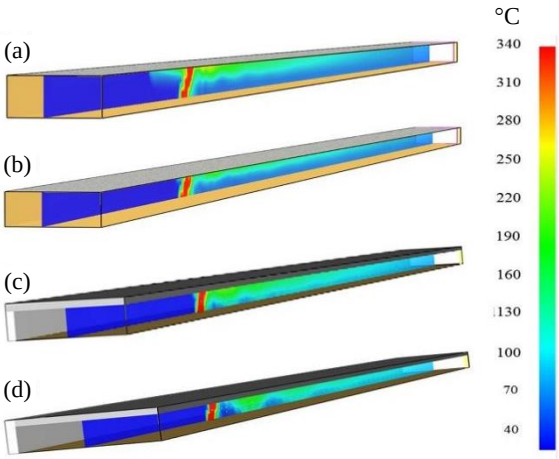

Fig. 18. Temperature distribution under four working conditions

Figure 18 shows that the temperature was highest at the center of the fire source, and the further away from the fire in the downstream direction, the lower the temperature was. Due to the existence of ventilation system, the temperature was lowest upstream of the fire source. The higher the location at the same distance, the higher the temperature. The highest temperature at the center of the fire source in conditions I and II reached 266 and 252 ℃, respectively, and the highest temperature at the center of the fire source in conditions III and IV reached 340 and 330 ℃, respectively.

Temperature distributions at different distances from the fire source center under various working conditions are shown in Fig. 19, which also illustrates that the closer the distance to the fire center, the higher the temperature. In the same wind speed, the larger the fire scale, the higher the temperature in the tunnel.

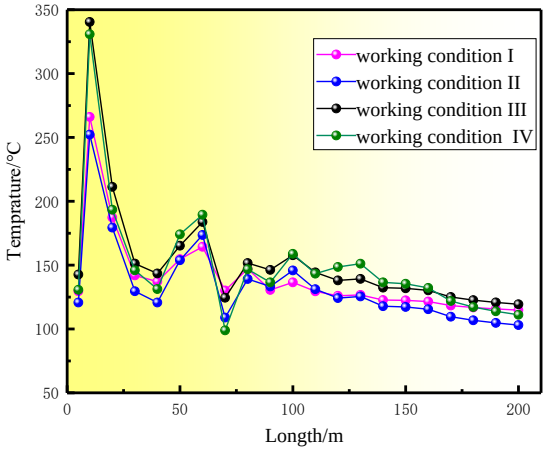

Fig. 19. Temperature comparison under four working conditions

The highest temperature among the four working conditions was working condition III, which reached 340 ℃. From 1 to 10 m, the temperature first rose sharply to the highest temperature and then fell sharply to 150 ℃. Due to the effect of air turbulence, there was a small temperature rise followed by a slow decrease to about 180 ℃. This comparison shows that the fire scale had a great influence on the temperature and the wind speed had a less significant influence on the fire temperature.

3.4. CO CONCENTRATION DISTRIBUTION IN FIRE

In the simulation process, CO concentration detectors were placed near the fire source point. CO concentration detectors were placed at 101, 105, and 110 m, followed by one every 10 m until 300 m. A total of 32 CO concentration detectors were placed 1.8 m above the ground to monitor the CO concentration. The maximum CO concentration over time was measured, and different CO concentration distributions were obtained for the four working conditions, as shown in Fig. 20.

Figure 20 shows that the closer the distance to the fire center, the higher the CO concentration. At the same wind speed, the larger the fire scale, the higher the concentration of CO. However, the downward trend was similar; CO concentration could be as high as 996 ppm under condition III, and the highest CO concentration point was 5 m away from the fire source center. Subsequently, the CO concentration rapidly decreased

between 5 and 10 m and then reached a stable level, always around 150 ppm. According to a comparison of the four working conditions, the CO concentration at the same position decreased with the increase in wind speed, and the maximum reduction was 282 ppm.

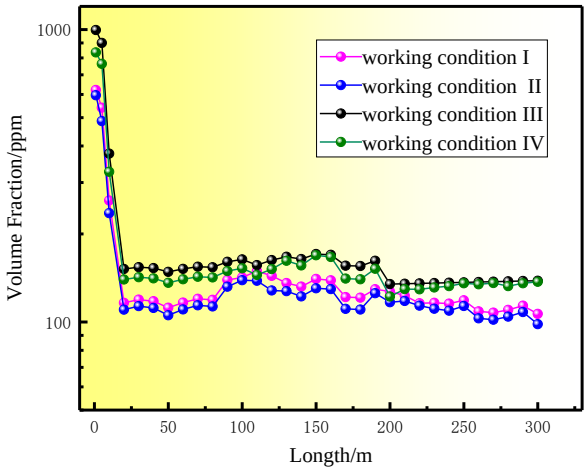

Fig. 20. CO distribution under four working conditions

4. CONCLUSIONS

1) The critical wind speed of a roadway in the fire period was found to be positively correlated with the fire scale to a certain extent, but the critical wind speed was found to not change after a certain limit. The critical wind speed of a medium fire was found to be about 2.3 m/s, and the critical wind speed of a large fire was found to be 3.1 m/s.
2) The time required for the smoke layer to descend to 1.8 m was found to be positively correlated with the distance between the location and the fire source and negatively correlated with the size of the fire source. Under the most unfavorable conditions, the smoke reached human breathing height at 15.11 s and 100 m away from the fire source. Therefore, the area near a fire source quickly becomes the most dangerous area after a roadway fire occurs.
3) The maximum temperature at the center of the fire source in conditions I and II reached 266 and 252 ℃, respectively, and the maximum temperature at the center of the fire source in conditions III and IV reached 340 and 330 ℃, respectively. At the 1–10 m stage, the temperature was found to rapidly increase and then slowly decrease. It could be seen from the comparison that the fire scale had a greater impact on the fire temperature than wind speed.

4) The highest CO concentration under the four working conditions was observed in working condition III at 996 ppm. The closer one is to the fire center, the larger the fire scale and the higher the CO concentration. The CO concentration was found rapidly decrease between 5 and 10 m and then to change little, remaining at about 150 ppm.

ACKNOWLEDGEMENTS

The authors appreciate the financial support of project No. 51974015 and No. 51474017 provided by the National Natural Science Foundation of China; project No. SMDPC202101 provided by the Key Laboratory of Mining Disaster Prevention and Control (Shandong University of Science and Technology); project No. FRF-IC-20-01 and No. FRF-IC-19-013 provided by the Fundamental Research Funds for the Central Universities; project No. 2018YFC0810601 provided by the National Key Research and Development Program of China; project No. WS2018B03 provided by the State Key Laboratory Cultivation Base for Gas Geology and Gas Control (Henan Polytechnic University), and project No. E21724 provided by the Work Safety Key Lab on Prevention and Control of Gas and Roof Disasters for Southern Coal Mines of China (Hunan University of Science and Technology).

REFERENCES

ADJISKI V., MIRAKOVSKI D., DESPODOV Z. et al., 2015, *Simulation and optimization of evacuation routes in case of fire in underground mines*, Journal of Sustainable Mining, 14(3), 133–143.

BAKHTIYARI S., AKBARI L.T., ASHTIANI M.J., 2017, *An investigation on fire hazard and smoke toxicity of epoxy FRP composites*, International Journal of Disaster Resilience in the Built Environment, 8(3), 230–237.

CHASKO L., CONTI R.S., LAZZARA C.P., 2005, *Fire response preparedness for underground mines*, National Institute for Occupational Safety and Health, 34(4), 196–208.

CHRIST G., 2015, *South African Mine Fire Heats Up Mine Safety Concerns*, EHS Today, 12, 204–205.

HANSEN R, INGASON H., 2013, *Heat release rate measurements of burning mining vehicles in an underground mine*, Fire Safety Journal, 61(11), 12–25.

HANSEN R., 2012, *Methodologies for calculating the overall heat release rate of a vehicle in an underground structure*, Fifth International Symposium on Tunnel Safety and Security, 6(5), 4–12.

HANSEN R., 2015, *Study of heat release rates of mining vehicles in underground hard rock mines*, School of Business Society and Engineering, 5(3), 101–106.

HANSEN R., 2021, *The passive fire protection of mining vehicles in underground hard rock mines*, Mining, Metallurgy and Exploration, 38(1), 609–622.

HANSEN R., MALMFLTENS, Brandkonsult., 2017, *Fire behavior of mining vehicles in underground hard rock mines*, International Journal of Mining Science and Technology, 27(4), 44–51.

HIRAI T., 2011, *Tunnel Ventilation Design and Build*, Journal of the Japan Society of Mechanical Engineers, 114, 160–162.

INGASON H., YING Z., 2010, *Model scale tunnel fire tests with longitudinal ventilation*, Fire Safety Journal, 45, 371–384.

INGASON H., LÖNNERMARK A., 2011, *Heat release rates in tunnel fires: a summary*, Thomas Telford, 42(6), 61–69.

INGASON H., YING Z.L., LNNERMARK A., 2015, *Tunnel Fire Dynamics*, New York.

KANG N., QIN Y., HAN X. et al., 2019, *Experimental study on heat release rate measurement in tunnel fires*, Fire and Materials, 43(4), 381–392.

KOCHEVSKY A.N., 2004, *Possibilities of simulation of fluid flows using the modern CFD software tools*, Physics.

MORIN M.A., 2001, *Underground hardrock mine design and planning: a system's perspective*, Dissertation Abstracts International, 52(4), 26–31.

MOUILLEAU Y., CHAMPASSITH A., 2009, *CFD simulations of atmospheric gas dispersion using the Fire Dynamics Simulator (FDS)*, Journal of Loss Prevention in the Process Industries, 22(3), 316–323.

OKA Y., OKA H., 2020, *Temperature and velocity distributions of a ceiling-jet along a flat-ceilinged tunnel with natural ventilation*, Fire Safety Journal, 112(2), 102969.

PERERA I.E., LITTON C.D., 2012, *Impact of Air Velocity on the Detection of Fires in Conveyor Belt Haulageways*, Fire Technology, 48(2), 405–418.

RAN G.Y., ZHANG G., ZHANG H. et al., 2020, *The Smoke Spread Rule under Different Longitudinal Wind Speed in the Case of Fire in a Blocked Tunnel*, IOP Conference Series Earth and Environmental Science, 544, 012006.

ROH J.S., HONG S.R., DONG H.K. et al., 2007, *Critical velocity and burning rate in pool fire during longitudinal ventilation*, Tunnelling and Underground Space Technology Incorporating Trenchless Technology Research, 22(3), 262–271.

SHEN T.S., HUANG Y.H., CHIEN S.W., 2008, *Using fire dynamic simulation (FDS) to reconstruct an arson fire scene*, Building and Environment, 43(6), 1036–1045.

SINGH A.K., SINGH R.V.K., SINGH M.P. et al., 2007, *Mine fire gas indices and their application to Indian underground coal mine fires*, International Journal of Coal Geology, 69(3), 192–204.

WANG H.Y., JOULAIN P., 2002, *Numerical simulation of wind-aided turbulent fires in a ventilated model tunnel*, Fire Safety Science – Proceedings of the Seventh International Symposium, 6(5), 161–172.

WANG W.C., JIANG Y.H., ZHANG B. et al., 2013, *Study on Heat Release Rate of Coal Combustion in Tunnel*, Safety in Coal Mines, 44(12), 40–42.

WANG Y., JIANG J., ZHU D., 2009, *Full-scale experiment research and theoretical study for fires in tunnels with roof openings*, Fire Safety Journal, 44(3), 339–348.

YAN G., FENG D., 2013, *Escape-Route Planning of Underground Coal Mine Based on Improved Ant Algorithm*, Mathematical Problems in Engineering, 11(1), 61–61.

YANG P., XUN T., WANG X., 2011, *Experimental study and numerical simulation for a storehouse fire accident*, Building and Environment, 46(7), 1445–1459.

YING Z.L., BO L., INGASON H., 2011, *Study of critical velocity and backlayering length in longitudinally ventilated tunnel fires*, Fire Safety Journal, 45(6–8), 361–370.

YING Z.L., INGASON H., 2012, *The maximum ceiling gas temperature in a large tunnel fire*, Fire Safety Journal, 48(1), 38–48.